Chinese Journal of
POLYMER SCIENCE

RESEARCH ARTICLE

https://doi.org/10.1007/s10118-026-3681-y
Chinese J. Polym. Sci.

Sodium Carboxymethyl Cellulose/Polypyrrole Nanoparticle-doped Conductive Hydrogel for Self-powered Flexible Strain Sensors and Signal Transmission

Jie He, Chang-Ning Hu, Zhou-Ya Yang, Hui Yang*, and Yin-Jie Peng*

School of Physics and Astronomy, China West Normal University, Nanchong 637009, China

Electronic Supplementary Information

Abstract Conductive hydrogels, with their excellent flexibility and tunable electrical conductivity, have shown broad application prospects in emerging fields such as flexible strain sensors and triboelectric nanogenerators (TENG). In this study, a conductive sodium carboxymethyl cellulose (CMC)/ polypyrrole (PPy)/polyacrylamide (PAM)(CPA) hydrogel was developed by integrating a CMC/PPy composite, synthesized *via in situ* polymerization, into a hydrophobic-associated polyacrylamide network. This hydrogel exhibits excellent mechanical properties, with a tensile strain as high as 1735%, demonstrating extremely high ductility and deformation capacity. The flexible sensor based on CPA hydrogel has a wide detection range (0%−500%) and can monitor the movements of various parts of the human body. In addition, the TENG assembled based on CPA hydrogel achieves stable electrical output performance, enabling it to power small wearable electronic devices and promote self-powered signal transmission, showing broad application prospects in the fields of intelligent human-machine interaction and wearable electronics.

Keywords Conductive hydrogel; Strain sensor; Triboelectric nanogenerators

Citation: He, J.; Hu, C. N.; Yang, Z. Y.; Yang, H.; Peng, Y. J. Sodium carboxymethyl cellulose/polypyrrole nanoparticle-doped conductive hydrogel for self-powered flexible strain sensors and signal transmission. *Chinese J. Polym. Sci.* https://doi.org/10.1007/s10118-026-3681-y

INTRODUCTION

The increasing demand for wearable smart electronics, driven by advancing globalization and digitalization, is pushing the perception layer of the Internet of Things (IoT) toward flexible and distributed architectures.[1−10] However, conventional electronic devices are constrained by their rigid form factors and dependence on external power sources. Triboelectric nanogenerators (TENGs) have emerged as a promising technology for converting ambient mechanical energy into electricity *via* triboelectrification and electrostatic induction, enabling self-powered and flexible integration.[11−13] Based on the structural design and relative motion of the friction layers, TENGs operate in four fundamental modes: vertical contact-separation, lateral sliding, freestanding triboelectric layer, and single-electrode mode.[14−17] Nevertheless, traditional rigid friction layers suffer from poor flexibility, low biocompatibility, and weak conformability to curved surfaces, restricting their use in flexible and bio-integrated applications, leading to mechanical failure over time.[18] Therefore, the development of novel functional materials with high triboelectric performance, environmental stability, and mechanical durability is essential for advancing the practical and widespread applications of TENGs.

Hydrogels are three-dimensional network soft materials containing water that feature multilevel pore structures, viscoelasticity, transparency, stretchability, and biocompatibility. In recent years, their applications have expanded from biomedical fields, such as tissue engineering, drug delivery, and wound dressings, to emerging areas, such as wearable electronics, soft robotics, and artificial intelligence sensing.[19−22] Therefore, hydrogels are regarded as ideal electrode materials for TENGs. However, their intrinsically low electrical conductivity severely restricts the effective transmission of charges, thereby limiting the practical performance of triboelectric nanogenerators.[23] Functional conductive components are usually introduced to enhance the electrical conductivity of the hydrogels. For instance, electrolyte salts (such as LiCl[24] and NaCl[25]) can achieve conductivity through ion migration mechanisms, but their conductivities are typically low and they are susceptible to environmental humidity, leading to unstable performance. Carbon-based materials (such as carbon nanotubes[26] and graphene[27]) and metal nanoparticles (such as metal nanoparticles[28]) can effectively construct conductive pathways, but their weak interface interaction with the hydrogel matrix can cause structural separation and a decline in conductive durability, restricting their long-term application in flexible electronic devices. In

* Corresponding authors, E-mail: sdlzyanghui@126.com (H.Y.)
E-mail: pyj1992263@hotmail.com (Y.J.P.)
Received February 5, 2026; Accepted March 18, 2026; Published online June 9, 2026

contrast, conductive polymers (such as PEDOT:PSS[29] and polypyrrole[30]) can form stable bonds with hydrogel networks through covalent or hydrogen bonding. These interactions significantly enhance electrical conductivity while improving mechanical stability and environmental adaptability, making them particularly suitable for flexible sensing and wearable electronics.

Conductive polymer-hydrogel composites synergistically combine the advantages of both components, yielding materials with tunable flexibility and enhanced electrical properties that hold great promise for advanced flexible electronic devices.[31–34] For instance, Sun *et al*. introduced pyrrole into a dual-crosslinked system based on hydroxyethyl cellulose macromonomer (HECM) and fabricated a cellulose composite hydrogel with high electrical conductivity and excellent mechanical self-reinforcement properties through *in situ* polymerization. This hydrogel can be used as an electrode in stretchable TENGs to achieve mechanical energy harvesting, human motion monitoring, and self-powered sensing.[35] Wang *et al*. incorporated Al (III) ions and polypyrrole into a carboxymethyl cellulose/poly(acrylic acid) system to prepare a multifunctional composite hydrogel with an efficient self-healing ability and high extensibility (1344%). This hydrogel achieved mechanical and electrical self-recovery through the synergy of dynamic metal coordination and hydrogen bonding, showing broad application prospects in electronic skin and wearable devices.[36] Therefore, in-depth research on the preparation methods for conductive hydrogels is of great significance for the development of flexible electronic devices.

This study presents a mild and efficient strategy for fabricating conductive hydrogels with uniformly dispersed nano-polypyrrole (PPy). Specifically, pyrrole monomers were polymerized in the presence of dissolved CMC, yielding a homogeneous PPy/CMC composite suspension *via* electrostatic interactions. Subsequently, acrylamide (AM) monomers were introduced and polymerized within this suspension to construct a CMC/PPy/PAM (CPA) hydrogel system. The resulting hydrogel exhibited excellent electrical conductivity and mechanical properties, enabling its application as a high-performance flexible sensor for real-time monitoring of human motion. Furthermore, a self-powered CPA-based triboelectric nanogenerator (CPA-TENG) is demonstrated, capable of efficiently transmitting electrical signals and powering small electronic devices such as LEDs and calculators.

EXPERIMENTAL

Materials

Pyrrole (Py), acrylamide (AM), sodium carboxymethyl cellulose (CMC), sodium dodecyl sulfate (SDS), lauryl methacrylate (LMA), 2,2'-azobis (2-methylpropionamidine) dihydrochloride (AIBA), iron (III) chloride hexahydrate ($FeCl_3{\cdot}6H_2O$), and hydrochloric acid (HCl) were purchased from Aladdin Inc. (Shanghai, China). Silicone rubber (Ecoflex) was acquired from Smooth-On Inc. (USA). Deionized water was used in all experiments. All chemicals were used as received.

Preparation of CMC/PPy Composite Suspension

Dissolve 1312.5 μL of Pyrrole in a 0.5 mol/L HCl solution (37.5 mL) and stirred for 5 min. Under magnetic stirring, pyrrole was slowly added to the CMC suspension (1 wt%, containing 0.5 g of CMC) and stirred until homogeneous. Then, 5.041 g of $FeCl_3{\cdot}6H_2O$ was dissolved in a 37.5 mL of 0.5 mol/L HCl and added dropwise to the mixed suspension of pyrrole and CMC. The mixture was stirred at room temperature for 1.5 h. After the reaction was complete, the resulting mixed suspension was placed in a dialysis bag and purified by dialysis in deionized water. Finally, the concentration of the obtained CMC/PPy composite suspension was adjusted to 1 wt% and stored at 4 °C in a refrigerator for subsequent use.

Preparation of CPA Hydrogel

First, 3 g of AM, 0.6 g of SDS and 0.3 g of LMA were successively added to 10 mL of CMC/PPy composite suspension. The mixture was stirred continuously for 30 min to ensure that all components were fully dissolved and mixed well. Then, 0.05 g of initiator AIBA was added to the above system and stirred for another 10 min. Subsequently, the solution was degassed *via* ultrasonic treatment and transferred to a mold composed of a pair of glass plates and a silicone gasket. Finally, the sample was placed in an oven at 60 °C for 1 h to obtain a CMC/PPy/PAM (CPA) hydrogel.

Preparation of CPA-TENG

Initially, components A and B of liquid Ecoflex (00-30) were mixed at a 1:1 weight ratio. The mixture was then poured into a prefabricated mold and cured at room temperature for 24 h. Subsequently, a CPA hydrogel with dimensions of 30 mm × 30 mm × 1.5 mm was placed onto the cured Ecoflex layer, with electrical connections established using conductive tape to serve as external electrodes. Uncured Ecoflex was then poured over the CPA hydrogel surface and allowed to cure at room temperature for an additional 24 h, resulting in final CPA-TENG device dimensions of 40 mm × 40 mm × 3 mm. For all TENG output measurements conducted using a linear motor, the effective contact area was maintained constant at 30 mm × 30 mm, corresponding to the dimensions of the hydrogel electrode. For the manual tapping tests, the effective contact area was determined using the finger contact region.

Material Characterizations and Electrical Measurement of CPA-TENG

The surface morphology of the lyophilized hydrogels was characterized by scanning electron microscopy (SEM, Inspect) at an accelerating voltage of 20 kV. Tensile tests were performed on the hydrogel samples at 25 °C using a universal testing machine (Model 5576) equipped with a 1 KN load cell, with a crosshead speed of 100 mm/min. Scanning hydrogels using a Raman spectrometer (Finder Vista) with an excitation wavelength of 532 nm and a scanning range from 3100 cm^{-1} to 500 cm^{-1}. Fourier-transform infrared spectroscopy (FTIR, Nicolet 6700, Thermo Fisher Scientific, USA) was employed to analyze the freeze-dried samples with a wavenumber range of 4000–400 cm^{-1} at 4 cm^{-1} resolution. For electromechanical measurements, a source meter (Keithley 2400) was connected to both ends of the CPA hydrogel, and the current-voltage characteristics were recorded during multiple cyclic stretching-relaxation processes. The CPA hydrogel was affixed to a volunteer's joint, with electrodes at both ends secured using adhesive tape, and connected to a source meter for electrical signal recording. To evaluate the output performance of the CPA-TENG, an external force was

applied *via* a linear motor (LinMot PS01-37×120-C) to establish periodic contact-separation motions with the device, while an electrometer (Keithley 2450) simultaneously measured the open-circuit voltage and short-circuit current.

RESULTS AND DISCUSSION

Formation Mechanism of CPA Hydrogel

The synthesis of the multifunctional hydrogels followed a sequential two-stage process, as illustrated in Fig. 1. First, a uniform and stable CMC/PPy composite suspension was prepared. The core of this strategy lies in the initial effective combination of PPy with carboxylate anions on the CMC chain through electrostatic interactions, thereby overcoming the dispersion problem caused by the inherent hydrophobicity of the PPy chain segments, which further enhances the hydrophilicity and dispersion stability of PPy in the aqueous phase, ultimately resulting in a uniform and stable CMC/PPy composite suspension.[37] Subsequently, in the second stage of hydrogel network formation, this pre-formed CMC/PPy complex is integrated into the hydrogel matrix through multiple physical interactions, achieving uniform *in situ* dispersion within the network and constructing a continuous interpenetrating conductive structure, thereby significantly enhancing the conductivity of the material.[38] In the preparation of hydrophobic CPA hydrogels, SDS was introduced as a surfactant to improve the dispersibility of LMA and stabilize the reaction system, promoting the formation of LMA micelles that act as physical crosslinking points.[39] The thermal decomposition of AIBA generates free radicals that initiate the polymerization of AM to form PAM long chains.[40,41] Meanwhile, the micelles containing LMA act as physical crosslinking points, connecting multiple PAM chains and reinforcing the three-dimensional network structure. The pre-prepared CMC/PPy complex was effectively embedded within and entangled by the in situ-formed PAM network, resulting in a structurally uniform black hydrogel with enhanced integrity and functionality (Fig. S1 in the electronic supplementary information, ESI).

Structure and Morphology

Control experiments were conducted to demonstrate the stabilizing role of CMC. As shown in Fig. 2(a), two suspensions were prepared under identical polymerization conditions: one with dissolved CMC (PPy/CMC) and the other without (pure PPy). Immediately after polymerization (Figs. 2a-I and 2a-II), the pure PPy suspension exhibited severe aggregation with visible black precipitates settling at the bottom and a clear supernatant (I), whereas the PPy/CMC suspension appeared as a homogeneous black solution without observable precipitation (II). After dialysis (Figs. 2a-III and 2a-IV), the pure PPy suspension remained aggregated, with distinct phase separation between the precipitate and supernatant (III). In contrast, the PPy/CMC suspension retained its homogeneous dispersion and showed no signs of aggregation or sedimentation even after dialysis (IV). These results demonstrate that dissolved CMC acts as an effective macromolecular stabilizer, preventing PPy aggregation during both the polymerization and subsequent processing steps.

Raman spectroscopy was used to confirm the presence of PPy in the hydrogels. As shown in Fig 2(b), characteristic bands at 929, 1045, and 1563 cm^{-1} corresponding to the C—H, C—N, and C=C stretching vibrations of PPy are observed in the CPA hydrogel, confirming successful incorporation of PPy.[42] Consequently, the regular enhancement of the characteristic band of PPy (1563 cm^{-1}) in Raman spectroscopy strongly proves that PPy was successfully and controllably integrated into the hydrogel network, and its dispersion state remained uniform within the tested concentration range (Fig. S2 in ESI).[43] FTIR spectroscopy provided additional evidence of the chemical structure of the composite. In the FTIR spectrum of the CPA hydrogel (Fig. S3 in ESI), the band at 1060 cm^{-1} is assigned to the in-plane deformation of N—H bonds on the pyrrole ring, and the peak at 1204 cm^{-1} corresponds to the C—N plane vibration of PPy, further confirming the successful integration of PPy.[44,45] Figs. 2(c) and 2(d) present scanning electron microscopy (SEM) images of CP_0A and CPA hydrogels, respectively. The CP_0A hydrogel exhibited a clear and open porous structure (Fig. 2c). In contrast, the three-dimensional porous network surface of the CPA hydrogel was uniformly covered with PPy nanoparticles, presenting a significantly roughened morphology and forming con-

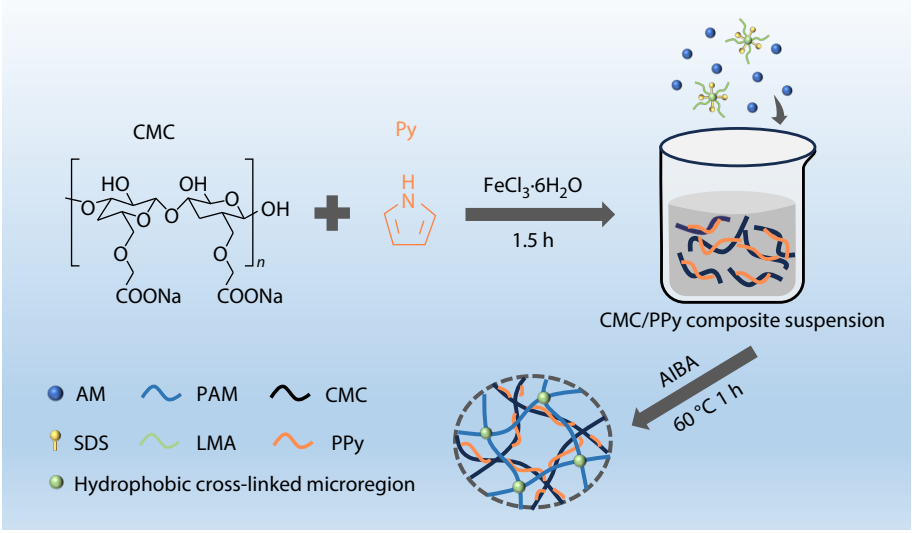

Fig. 1 Fabrication process of the composite hydrogel.

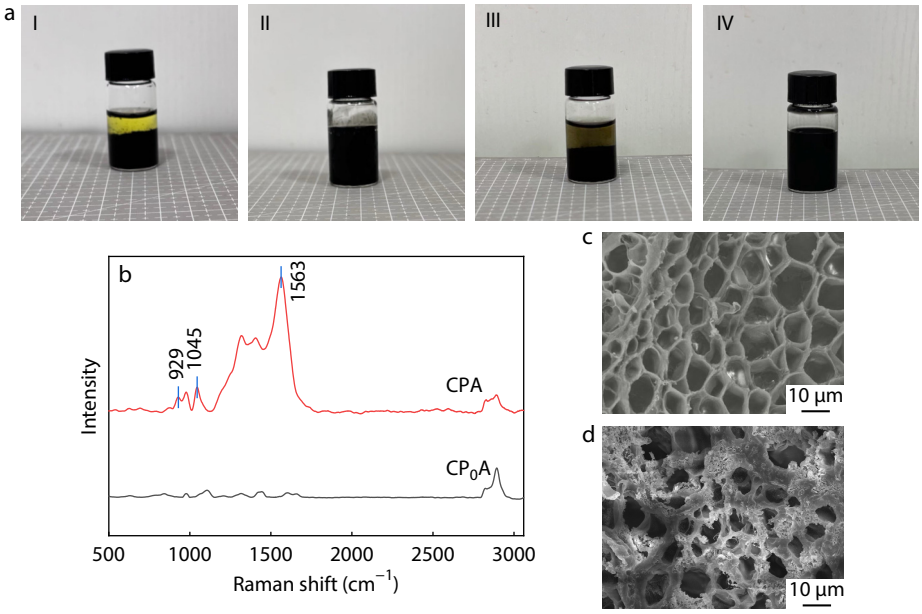

Fig. 2 (a) Photographs of PPy suspensions: (I, III) without CMC; (II, IV) with CMC. (I, II) Immediately after polymerization; (III, IV) After dialysis; (b) Raman spectra of CP_0A and CPA hydrogels; SEM images of the cross-sections of (c) CP_0A hydrogel and (d) CPA composite hydrogel after freeze-drying and freeze-fracture treatment.

tinuous conductive pathways (Fig. 2d and Fig. S4 in ESI). These structural differences demonstrate that the incorporation of PPy effectively constructs a conductive network throughout the hydrogel, providing direct microscopic evidence of its significantly enhanced electrical properties.

Mechanical Properties

The mechanical properties of CPA hydrogels were systematically characterized. As shown in Fig. 3(a), the hydrogel exhibited an excellent tensile deformation ability. Additionally, it possesses outstanding flexibility and deformability, with various deformation modes, such as bending, twisting, and even knotting (Fig. 3b). Notably, the CPA hydrogel also demonstrated high mechanical strength, successfully supporting a 200 g weight without failure (Fig. 3c). The uniformly distributed CMC/PPy effectively integrates with the polymer network through hydrogen bonding between the amino groups of PAM and carboxyl groups of CMC.[46] This integration facilitated efficient energy dissipation during deformation, significantly improving the toughness of the CPA hydrogel. To further investigate the influence of the CMC/PPy composite suspension concentration on the mechanical properties of the hydrogel, we conducted tensile performance tests on the CPA hydrogels. As shown in Fig. 3(d), the typical stress-strain curve of the CPA hydrogel indicates that its mechanical properties mainly depend on the CMC/PPy content. As the content increased, the breaking stress exhibited an initial upward trend. When the content was 0.1%, the hydrogel exhibited optimal tensile performance, with a stress of 472.22 kPa and a breaking elongation of 1735%. This improvement was attributed to the increased polymer chain density and crosslinking points resulting from the higher CMC concentration, which strengthened the hydrogen bonding interactions and led to a more compact network structure. However, excessive crosslinking may impair the network's ability to dissipate energy effectively during deformation.[47] Consequently, when the CMC/PPy content reached 0.15%, the tensile strength increased to 494.23 kPa, whereas the elongation at break decreased to 1683% (Figs. 3e and 3f).[48] Thus, CPA composite hydrogels with a CMC/PPy composite suspension concentration of 0.1% were used in subsequent studies.

The critical role of hydrophobic associations in the mechanical properties of CPA hydrogels was verified using a control experiment. As shown in Fig. S5 (in ESI), the hydrogel prepared without LMA (denoted as CP_0A-LMA) was mechanically weak and fragile, failing to form a self-standing structure or peel intact from the glass mold. In contrast, the CPA hydrogel containing LMA exhibited excellent mechanical integrity and flexibility. This result directly confirms that the LMA-derived hydrophobic associations serve as essential physical crosslinking points for network formation. The energy dissipation capability provided by these physical crosslinks was further demonstrated by cyclic loading-unloading tests.[49] Fig. 3(g) shows the curves of 10 consecutive loading-unloading cycles of the CPA hydrogel at 500% strain. Obvious hysteresis loops appear in each cycle, with the loop area decreasing after the first cycle. Specifically, the first cycle exhibited dissipated energy of approximately 44 kJ/m^3. Over the subsequent nine cycles (Cycles 2–10), the dissipated energy decreased significantly and stabilized at an average value of approximately 13 kJ/m^3, corresponding to an energy-dissipation efficiency of approximately 30% relative to the first cycle (Fig. S6 in ESI). This indicates that the internal reversible sacrificial bonds (such as hydrogen bonds or hydrophobic associations) were restructured after the first stretch, leading to a stabilized energy-dissipation efficiency.[50] This mechanism effectively inhibits crack propagation and endows the material with an excellent toughness and tear resistance. Fig. 3(h) shows the cyclic responses of CPA hydrogels at different strains (100%–500%). All curves exhibited pronounced hysteresis, with the hysteresis area increasing progressively with

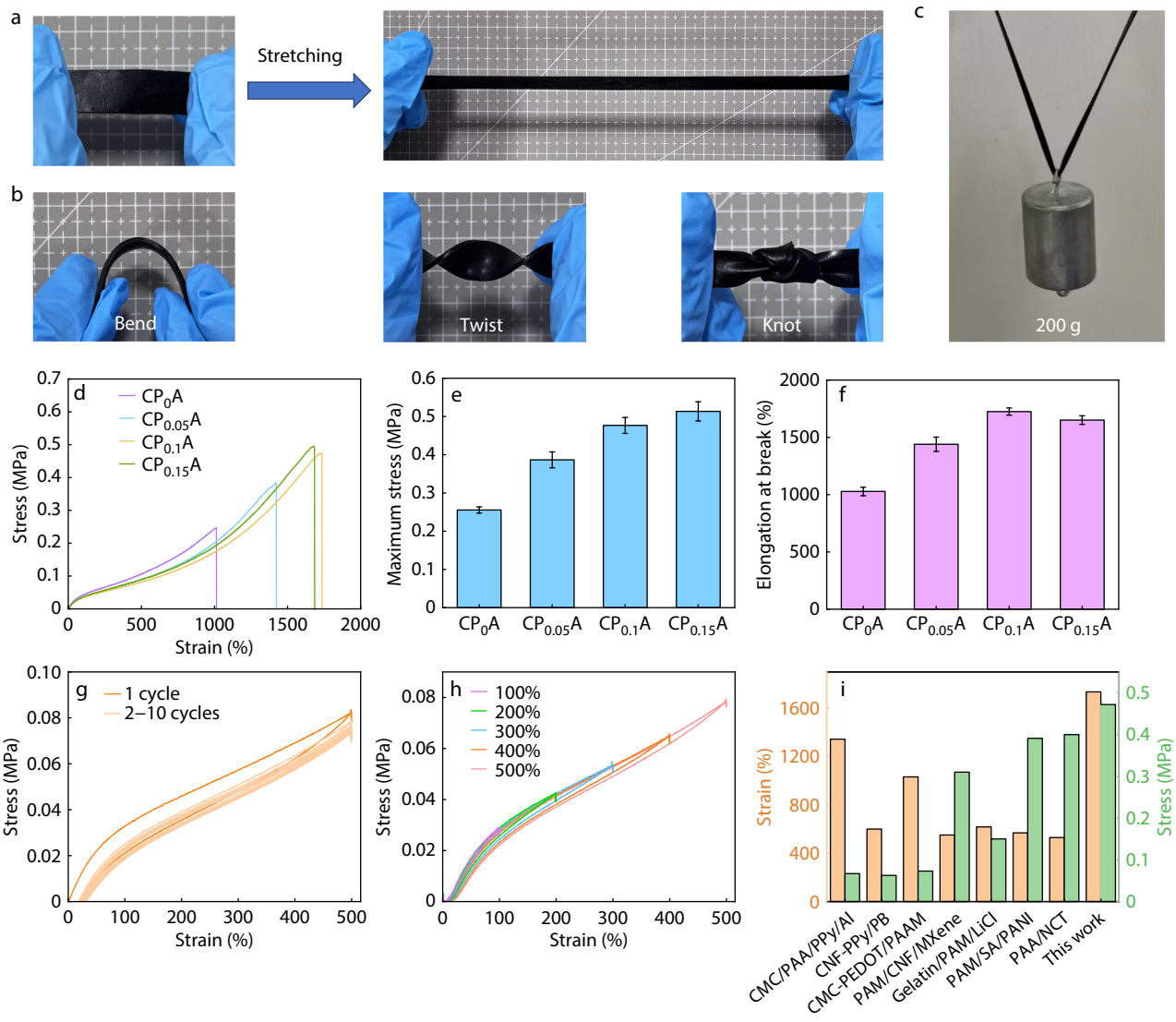

Fig. 3 Mechanical properties of the CPA hydrogel. (a) Images of the CPA hydrogel in a stretched state; (b) Images of the hydrogel in bent, twisted, and knotted states. (c) Image depicting CPA hydrogel supporting a 200 g load; (d) Stress-strain curves, (e) maximum stress, and (f) elongation at break of hydrogels with different CMC/PPy composite suspension contents; (g) Cyclic loading-unloading stress-strain curves of the CPA hydrogel at a strain of 500%; (h) Loading-unloading stress-strain curves of the CPA hydrogel at strain levels of 100%, 200%, 300%, 400%, and 500%; (i) Comparison of mechanical properties of CPA hydrogel with other high-strength hydrogels (The corresponding materials for each reference are listed in Table S8 in ESI).

strain, indicating strain-dependent energy dissipation and stable elastic recovery. These cyclic test results consistently demonstrated that the hydrogel exhibited good repeatable deformability and elasticity. Moreover, the CPA hydrogel exhibited superior compressive properties, which is consistent with its tensile performance (Fig. S7 in ESI). Together, these attributes enable the CPA hydrogel to demonstrate outstanding comprehensive mechanical properties relative to other high-strength hydrogels (Fig. 3i).[36,51–56] The selection of these reference materials is justified by their representation of diverse toughening strategies, including double-network, nanocomposite, and ionic crosslinking mechanisms, thereby establishing a robust benchmark for evaluating the performance of our CPA hydrogel.

Electrical Properties of CPA Hydrogel and Their Application as Strain Sensors

The CPA hydrogel exhibited outstanding electrical conductivity, making it highly suitable for use as a flexible strain sensor for monitoring human movement. The conductivities of the prepared composite hydrogels were measured quantitatively using a digital source meter. As shown in Fig. 4(a), the electrical conductivity increased progressively with increasing CMC/PPy composite suspension concentration, reaching 0.887 S/m at a concentration of 0.1%. This trend is attributed to the formation of a more continuous and dense conductive pathway provided by the well-dispersed PPy chains within the polymer network.[57] The sensitivity of a hydrogel-based strain sensor can be quantified by the gauge factor (GF), which is defined as the ratio of the relative resistance change ($\Delta R/R_0$) to the applied strain.[58–60] As

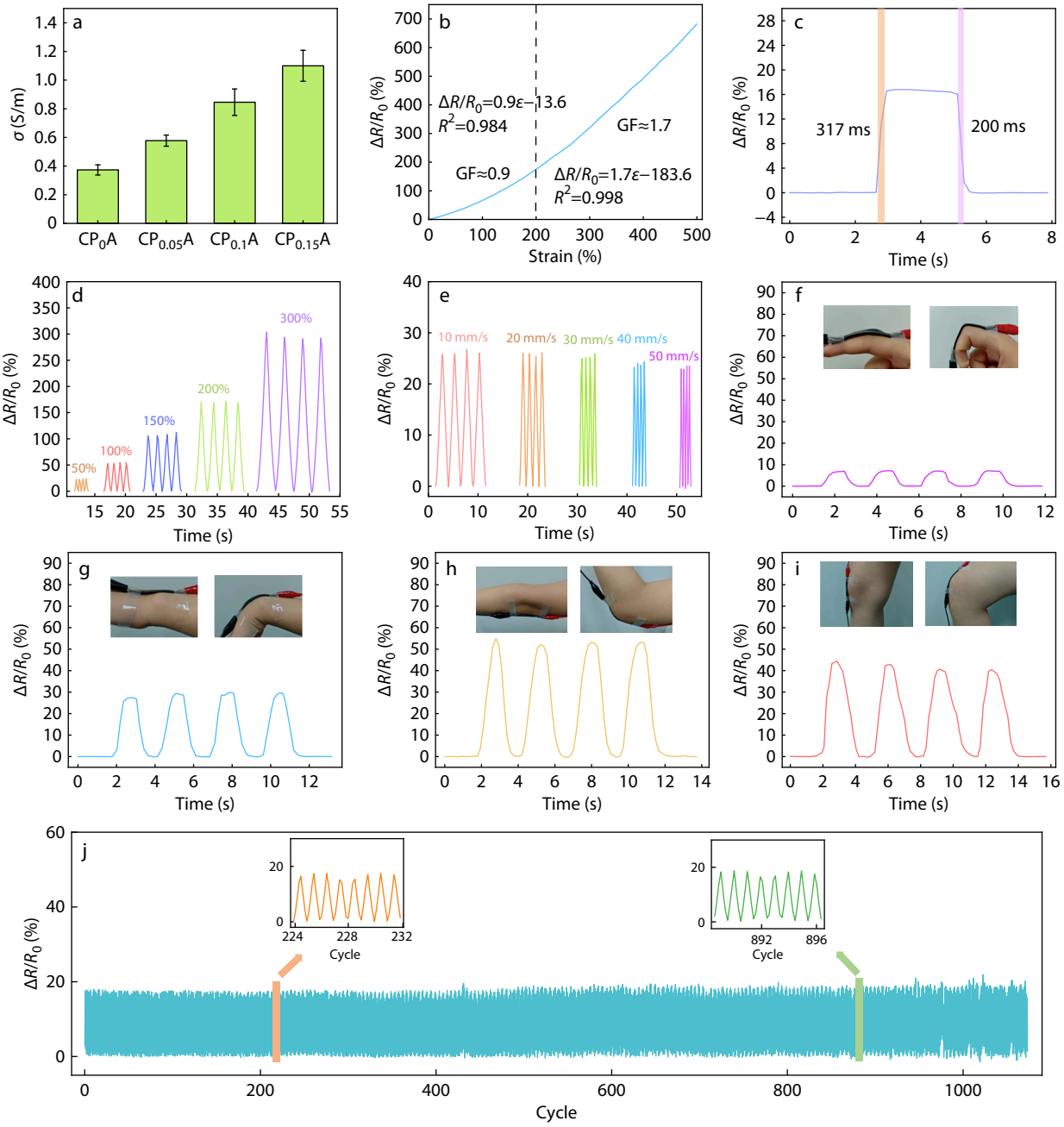

Fig. 4 (a) Conductivity of hydrogels with different contents of CMC/PPy; (b) Sensitivity curve of CPA hydrogel; (c) Response time and recovery time of CPA hydrogel under stretching conditions; $\Delta R/R_0$ response of CPA hydrogel at (d) various strains and (e) various stretching rates. (f–i) Real-time signals from the CPA hydrogel as a strain sensor; (j) Cyclic stability of the CPA hydrogel sensor over 1000 cycles at 50% strain.

shown in Fig 4(b), $\Delta R/R_0$ increased monotonically with strain. The GF can be divided into two linear response regions by linearly fitting the experimental data. In the strain range of 0%–200%, the linear regression equation is $\Delta R/R_0 = 0.9\varepsilon - 13.6$ (R^2=0.984), yielding a GF of approximately 0.90. In the strain range of 200%–500%, the linear regression equation is $\Delta R/R_0 = 1.7\varepsilon - 183.6$ (R^2=0.998), corresponding to a GF of about 1.70. The high correlation coefficients (R^2>0.98) indicate the excellent linearity of the sensor response in both regions. As shown in Fig 4(c), the hydrogel exhibited excellent response characteristics to dynamic mechanical strain. Under 100% applied strain (stretching rate of 100 mm/min), the response and recovery times were approximately 317 and 200 ms, respectively. Such rapid response and recovery performance indicate that the hydrogel is suitable for real-time monitoring of high-frequency dynamic strain. Figs. 4(d) and 4(e) show the responses of the hydrogels to different tensile strains and strain rates, respectively. The CPA hydrogel maintained a stable signal output across a strain range of 50%–300% and a strain rate range of 10–50 mm/s. These results demonstrate that the CPA hydrogel strain sensor possesses excellent sensing properties, such as a wide response range and high sensitivity, making it suitable for monitoring human

movement.

Furthermore, its favorable mechanical properties make it an ideal candidate for wearable sensing applications. Based on these attributes, we integrated the hydrogel into a wearable flexible strain sensor and attached it to the human skin to monitor joint movements in real time. As shown in Figs. 4(f)–4(i), the sensor conformably adheres to various joints, such as fingers, wrists, elbows, and knees, reliably reflecting movement through real-time electrical signal acquisition. To evaluate the sensing performance stability of the CPA hydrogel sensor, Fig. 4(j) shows the highly reproducible $\Delta R/R_0$ signal curves recorded during 1000 consecutive stretching–releasing cycles at a constant strain of 50%. This demonstrated the excellent cyclic stability of the sensor under dynamic operation. Such robust performance is attributed to the unique network architecture and stable conductive design of the CPA hydrogel, which enables it to withstand repeated mechanical strain without structural degradation, thereby ensuring a consistent and reliable signal output for monitoring periodic physiological activities or mechanical motions.

Electrical Output Performance of CPA-TENG

A triboelectric nanogenerator (TENG) is a device capable of efficiently converting mechanical energy into electrical energy.[61] Owing to its excellent mechanical properties and flexibility, CPA hydrogel serves as an ideal soft electrode material for constructing TENGs. Fig. 5(a) shows the structural design of the sandwich-structured single-electrode CPA-TENG, in which the CPA hydrogel is encapsulated between two layers of Ecoflex elastic medium, functioning as both the triboelectric layer and electrode connecting the external circuit. As shown in Fig. 5(b), the working principle of the CPA-TENG relies on the coupled mechanisms of the triboelectric effect and electrostatic induction. Specifically, (i) when nitrile rubber comes into contact with Ecoflex, electron transfer occurs at the interface owing to the difference in electron affinities. Electrons migrate from Ecoflex (lower electron affinity) to nitrile rubber (higher electron affinity), resulting in a positively charged Ecoflex surface and negatively charged nitrile rubber surface. (ii) During separation, the positive charge on the Ecoflex layer induced a negative charge on the adjacent side of the CPA hydrogel *via* electrostatic induction. To maintain electrical neutrality, free electrons flow from the ground to the hydrogel surface, generating an electrical signal. (iii) As the separation distance increased, the induced charge on the hydrogel surface gradually reached saturation, sufficiently shielding the positive electric field of the Ecoflex layer. At this point, the electrons in the external circuit stop flowing and the current drops to zero. (iv) When nitrile rubber approaches Ecoflex again, the negative charge on its surface drives electrons from the hydrogel surface through an external circuit to the ground, producing a reverse electrical signal.[62] The above process repeats in a periodic contact-separation motion, thereby continuously generating alternating current signals.

Various materials have been explored as potential contact layers for TENGs in practical applications. To identify the most suitable candidate, we systematically evaluated the electrical output performance of several common materials including polyethylene (PE), paper, polyimide (PI), and nitrile rubber. As shown in Fig. 5(c), nitrile rubber generated the highest output voltage of approximately 80 V, whereas PE produced the lowest output voltage of approximately 30 V. Based on these results, we selected nitrile rubber as the friction layer material for the CPA-TENG for subsequent experimental studies. Figs. 5(d) and 5(e) show the open-circuit voltage (V_{OC}) and short-circuit current (I_{SC}) measured for the CPA-TENG at different contact-separation frequencies. The results indicated that as the operating frequency increased, the I_{SC} significantly increased, mainly because of the enhanced charge transfer rate within the hydrogel electrodes. In contrast, V_{OC} remained relatively stable at different frequencies. As shown in Fig. 5(f), multi-finger tapping (*e.g.*, two or three fingers) of the CPA-TENG generated higher output voltages than single-finger tapping, indicating a positive correlation between the increase in the contact area and the enhancement of the output voltage. To systematically assess the mechanical durability and output stability of the CPA-TENG, long-term continuous contact–separation cycling tests were conducted. As shown in Fig. 5(g), after 30 min of continuous operation at a frequency of 3 Hz, the device maintained stable electrical output performance without significant attenuation. The results demonstrate that the CPA-TENG possesses excellent cyclic durability and long-term operational stability, rendering it suitable for continuous mechanical energy-harvesting and self-powered sensing applications in practical environments.

Owing to its efficient energy conversion capability and stable output characteristics, the CPA-TENG holds great promise as a core unit in self-powered systems capable of supplying sustainable energy to low-power electronic devices or distributed sensor networks. To evaluate the output performance of the CPA-TENG in self-powered systems, it was connected to a rectifier circuit containing an LED, capacitor, and calculator (Fig. 6a). As shown in Fig. 6(b) and Video S1 (in ESI), the CPA-TENG successfully lit the LED, confirming its ability to power the LED. The charging performance of the CPA-TENG was evaluated under various capacitance conditions. Fig. 6(c) highlights its advantages in energy harvesting and storage, making it suitable for powering small electronic devices. Furthermore, by connecting the calculator to this rectifier circuit, the electrical energy generated by the CPA-TENG (effective contact area: 30 mm × 30 mm, driven by a linear motor) could maintain the normal operation of the calculator (Fig. 6d and Video S2 in ESI), further demonstrating its practical applicability as a sustainable energy source. To evaluate the output performance of the CPA-TENG quantitatively, we measured the output voltage and current under various external load resistances and calculated the corresponding power density. As shown in Fig. S9 (in ESI), the output voltage increased with increasing load resistance, whereas the current exhibited the opposite trend. The power density reached a maximum value of 18.2 μW/mm^2 at a matching load resistance of 10 MΩ, demonstrating the efficient energy-harvesting capability of the CPA-TENG.

Notably, the CPA-TENG has self-powering characteristics and can be applied to communication and information encryption systems without reliance on external power sources. As shown in Figs. 6(e)–6(g), this system uses Morse code for signal encoding, where short V_{OC} signals represent "dots" and continuous V_{OC} signals represent "dashes". Different combinations of these signals encode specific letters, such as "HELP"

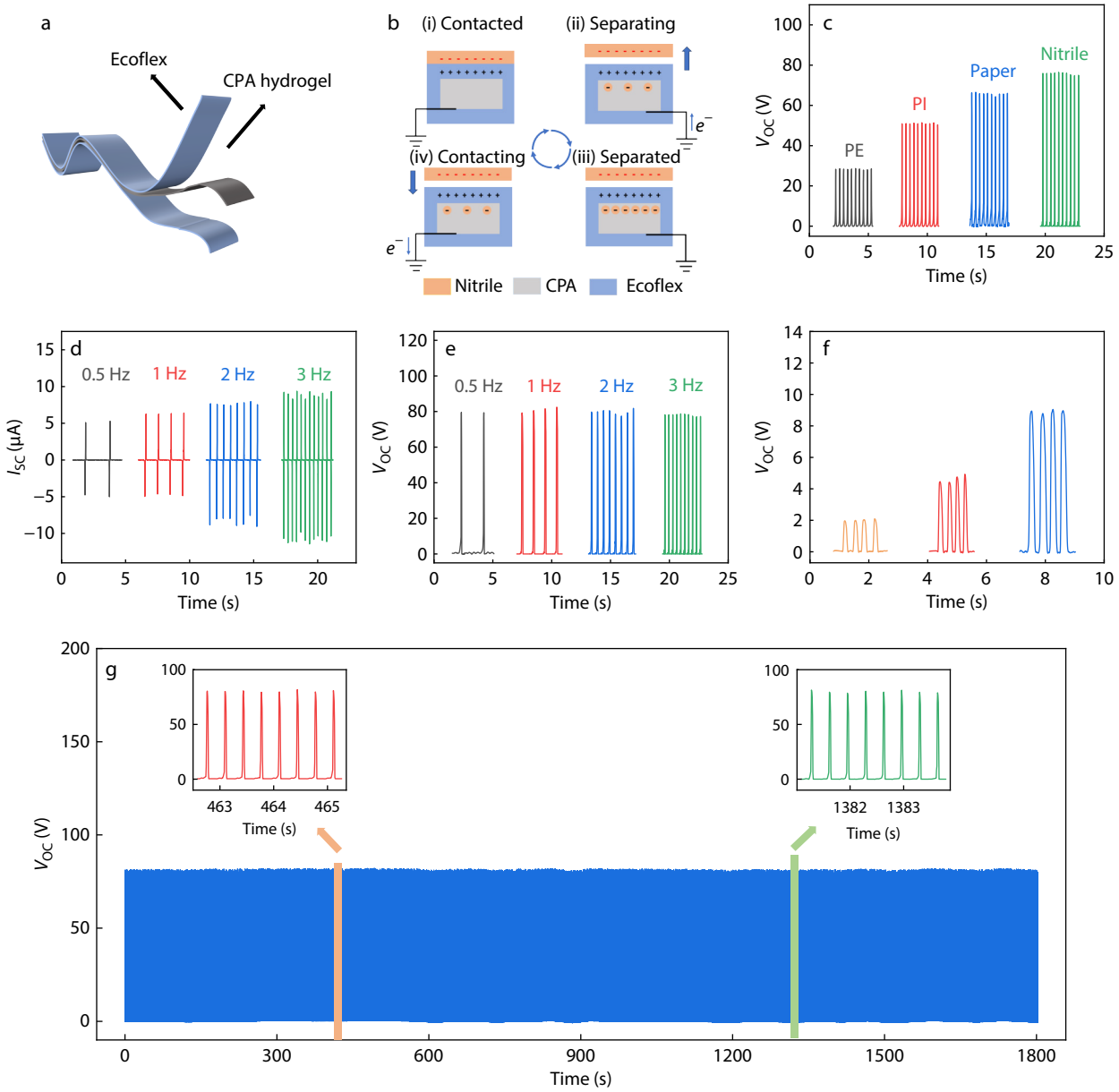

Fig. 5 (a) Schematic diagram of the CPA-TENG; (b) Working principle of the CPA-TENG; (c) Open-circuit voltage of the CPA-TENG with different triboelectric materials; (d) Short-circuit current and (e) open-circuit voltage of the CPA-TENG at different tapping frequencies; (f) Open-circuit voltage of the CPA-TENG when tapped with one, two, and three fingers; (g) Open-circuit voltage performance of the CPA-TENG after prolonged operation.

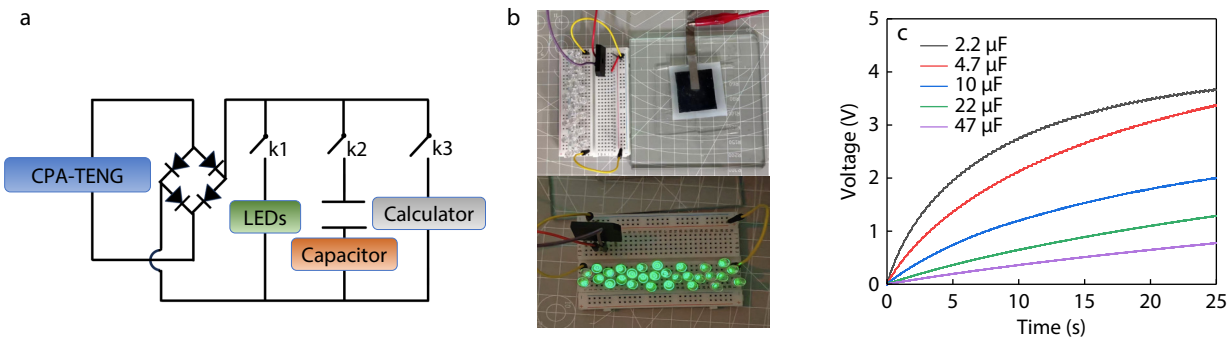

https://doi.org/10.1007/s10118-026-3681-y

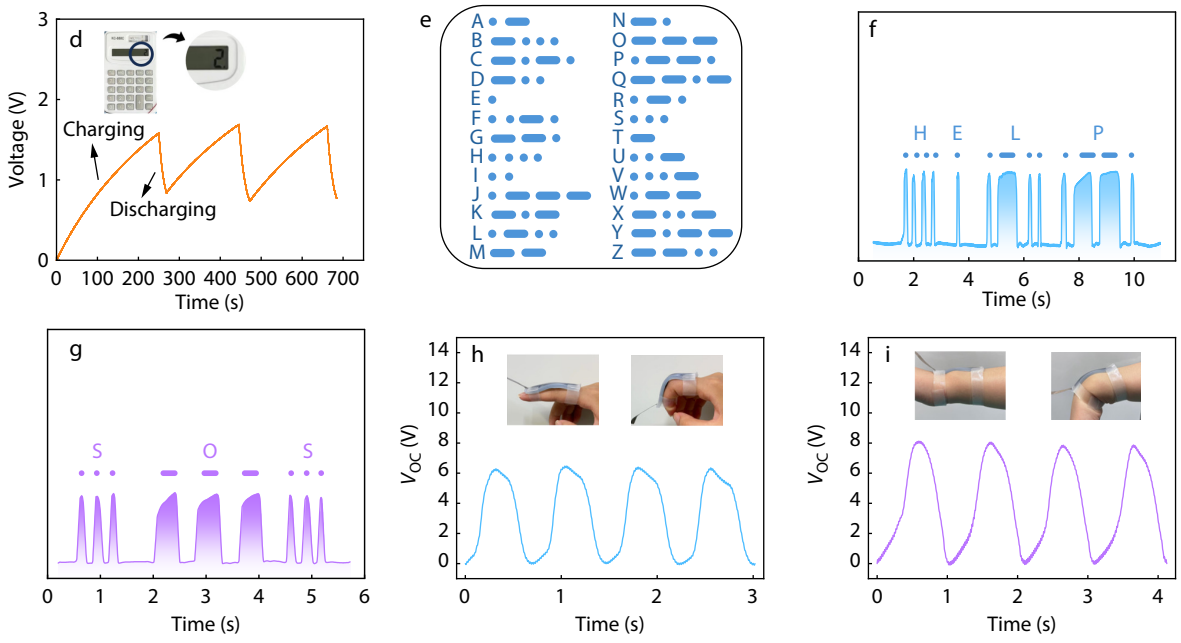

Fig. 6 (a) Circuit configuration of the CPA-TENG with an external load; (b) Image showing an LED illuminated by tapping the CPA-TENG with a hand; (c) Charging behavior of the CPA-TENG with different commercial capacitors (1–47 μF); (d) Three charging–discharging cycles of the CPA-TENG powering a calculator; (e–g) Transmission of Morse code by adjusting tapping duration on the CPA-TENG; (h, i) Real-time response of the CPA-TENG as a self-powered strain sensor.

and "SOS." This demonstration highlights the potential of the device for applications in self-powered communications and information security. Additionally, the CPA-TENG exhibited excellent flexibility and adhesion, generating distinct electrical signal responses upon mechanical deformation (*e.g.*, stretching, bending, or pressing). This feature enables it to be closely attached to the human skin surface (*e.g.*, fingers and wrists) and serves as a self-powered sensor to monitor various human motion states in real time (Figs. 6h and 6i).

CONCLUSIONS

In summary, CPA composite hydrogels with uniformly dispersed nano-PPy structures were successfully prepared. The hydrophobic association and multiple hydrogen bond interactions within the hydrogels endowed them with excellent mechanical properties. Furthermore, the introduction of CMC/PPY composites effectively built a conductive network, conferring hydrogels with good electrical conductivity. Based on these characteristics, hydrogels can be used as high-performance flexible sensors for human motion monitoring. Therefore, this study further combined CPA hydrogels with Ecoflex to construct a CPA-TENG. This device exhibits efficient energy harvesting capabilities and highly stable electrical output performance and is capable of continuously powering small electronic devices such as LED lights and calculators. In addition, based on a programmable coding strategy, this TENG can achieve information transmission functions in a self-driven state. These characteristics indicate that this research has broad application prospects in cutting-edge fields, such as medical electronic monitoring and intelligent human-machine interaction.

Conflict of Interests

The authors declare no interest conflict.

Electronic Supplementary Information

Electronic supplementary information (ESI) is available free of charge in the online version of this article at http://doi.org/10.1007/s10118-026-3681-y.

Data Availability Statement

Data supporting the findings of this study are available from the corresponding author upon reasonable request.

REFERENCES

1 Luo, X.; Zhu, L.; Wang, Y. C.; Li, J.; Nie, J.; Wang, Z. L. A flexible multifunctional triboelectric nanogenerator based on MXene/PVA hydrogel. *Adv. Funct. Mater.* **2021**, *31*, 2104928.
2 Torres, F. G.; Troncoso, O. P.; De-la-Torre, G. E. Hydrogel-based triboelectric nanogenerators: Properties, performance, and applications. *Int. J. Energy Res.* **2022**, *46*, 5603–5624.
3 Sun, E.; Wang, Y.; Zhang, Z.; Chen, Y.; Shoaib, M.; Cao, X.; Wang, N. Hydrogel-Based Triboelectric Nanogenerators: Current Progress and Future Perspectives. *Adv. Funct. Mater.* **2025,** e11382.
4 Jing, X.; Li, H.; Mi, H. Y.; Feng, P. Y.; Tao, X.; Liu, Y.; Liu, C.; Shen, C. Enhancing the performance of a stretchable and transparent triboelectric nanogenerator by optimizing the hydrogel ionic electrode property. *ACS Appl. Mater. Interfaces* **2020**, *12*, 23474–23483.
5 Zhang, H.; Li, D.; Ren, Y.; Han, L.; Teng, H. Instant-healing hydrogel-based triboelectric nanogenerator fornon-contact

Graphical Abstract

Sodium Carboxymethyl Cellulose/Polypyrrole Nanoparticle-doped Conductive Hydrogel for Self-powered Flexible Strain Sensors and Signal Transmission

Jie He, Chang-Ning Hu, Zhou-Ya Yang, Hui Yang, and Yin-Jie Peng

China West Normal University

A high-performance conductive hydrogel is prepared *via in situ* incorporation of a CMC/PPy composite into a hydrophobic polyacrylamide network. It combines excellent mechanics with a wide sensing range, enabling wearable strain sensing, self-powered sensing, and Morse code transmission.

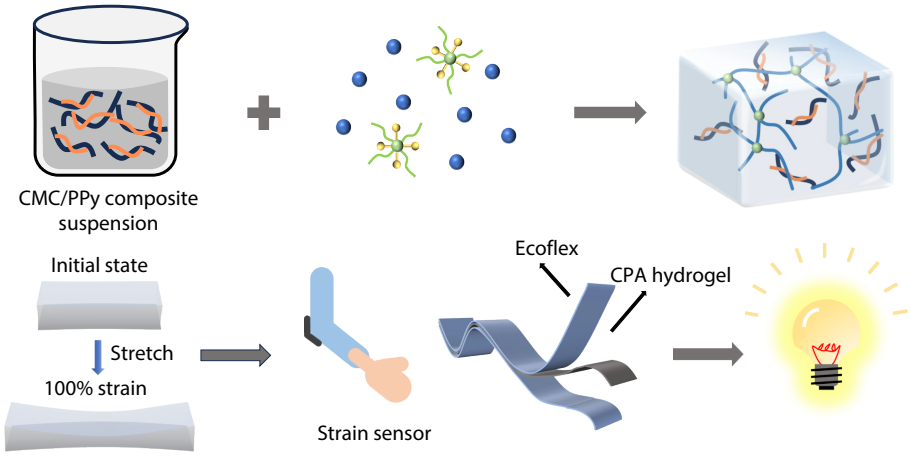

Chinese J. Polym. Sci., 2026 *https://doi.org/10.1007/s10118-026-3681-y*

sensing and energy harvesting. *Chem. Eng. J.* **2025**, *511*, 161803.
6 Zhao, L.; Fang, C.; Qin, B.; Yang, X.; Poechmueller, P. Conductive dual-network hydrogel-based multifunctional triboelectric nanogenerator for temperature and pressure distribution sensing. *Nano Energy* **2024**, *127*, 109772.
7 Rahman, M. T.; Rahman, M. S.; Kumar, H.; Kim, K.; Kim, S. Metal-organic framework reinforced highly stretchable and durable conductive hydrogel-based triboelectric nanogenerator for biomotion sensing and wearable human-machine interfaces. *Adv. Funct. Mater.* **2023**, *33*, 2303471.
8 Zhang, H.; Zhang, D.; Wang, Z.; Xi, G.; Mao, R.; Ma, Y.; Wang, D.; Tang, M.; Xu, Z.; Luan, H. Ultrastretchable, self-healing conductive hydrogel-based triboelectric nanogenerators for human–computer interaction. *ACS Appl. Mater. Interfaces* **2023**, *15*, 5128–5138.
9 Long, Y.; Wang, Z.; Xu, F.; Jiang, B.; Xiao, J.; Yang, J.; Wang, Z. L.; Hu, W. Mechanically Ultra-Robust, elastic, conductive, and Multifunctional hybrid Hydrogel for a triboelectric nanogenerator and flexible/wearable sensor. *Small* **2022**, *18*, 2203956.
10 Liu, Y.; Wong, T. H.; Huang, X.; Yiu, C. K.; Gao, Y.; Zhao, L.; Zhou, J.; Park, W.; Zhao, Z.; Yao, K. Skin-integrated, stretchable, transparent triboelectric nanogenerators based on ion-conducting hydrogel for energy harvesting and tactile sensing. *Nano Energy* **2022**, *99*, 107442.
11 Lei, T.; Wang, Y.; Zhang, Q.; Wang, H.; Duan, X.; Yan, J.; Xia, Z.; Wang, R.; Shou, W.; Li, X. Ultra-stretchable and anti-freezing ionic conductive hydrogels as high performance strain sensors and flexible triboelectric nanogenerator in extreme environments. *Nano Energy* **2024**, *126*, 109633.
12 Wu, Y.; Luo, Y.; Cuthbert, T. J.; Shokurov, A. V.; Chu, P. K.; Feng, S. P.; Menon, C. Hydrogels as soft ionic conductors in flexible and wearable triboelectric nanogenerators. *Adv. Sci.* **2022**, *9*, 2106008.
13 Patnam, H.; Graham, S. A.; Manchi, P.; Paranjape, M. V.; Yu, J. S. Single-electrode triboelectric nanogenerators based on ionic conductive hydrogel for mechanical energy harvester and smart touch sensor applications. *ACS Appl. Mater. Interfaces* **2023**, *15*, 16768–16777.
14 Wang, Z.; Liu, Z.; Zhao, G.; Zhang, Z.; Zhao, X.; Wan, X.; Zhang, Y.; Wang, Z. L.; Li, L. Stretchable unsymmetrical piezoelectric BaTiO3 composite hydrogel for triboelectric nanogenerators and multimodal sensors. *ACS Nano* **2022**, *16*, 1661–1670.
15 Luo, Y.; Yu, M.; Zhang, Y.; Wang, Y.; Long, L.; Tan, H.; Li, N.; Xu, L.; Xu, J. Highly sensitive strain sensor and self-powered triboelectric nanogenerator using a fully physical crosslinked double-network conductive hydrogel. *Nano Energy* **2022**, *104*, 107955.
16 Wang, Z.; Yao, S.; Wang, S.; Liu, Z.; Wan, X.; Hu, Q.; Zhao, Y.; Xiong, C.; Li, L. Self-powered energy harvesting and implantable storage system based on hydrogel-enabled all-solid-state supercapacitor and triboelectric nanogenerator. *Chem. Eng. J.* **2023**, *463*, 142427.
17 Hu, L.; Chee, P. L.; Sugiarto, S.; Yu, Y.; Shi, C.; Yan, R.; Yao, Z.; Shi, X.; Zhi, J.; Kai, D. Hydrogel-based flexible electronics. *Adv. Mater.* **2023**, *35*, 2205326.
18 Xie, B.; Ma, Y.; Luo, N.; Chen, Y.; Liu, Y.; Nie, K.; Jia, Y.; Yin, R.; Liu, Y.

Triple network hydrogel-based structure triboelectric nanogenerator for human motion detection and structural health monitoring. *Nano Energy* **2024**, *130*, 110095.
19 Li, R.; Xu, Z.; Li, L.; Wei, J.; Wang, W.; Yan, Z.; Chen, T. Breakage-resistant hydrogel electrode enables ultrahigh mechanical reliability for triboelectric nanogenerators. *Chem. Eng. J.* **2023**, *454*, 140261.
20 Wang, C.; Niu, H.; Shen, G.; Li, Y. Self-healing hydrogel-based triboelectric nanogenerator in smart glove system for integrated drone safety protection and motion Control. *Adv. Funct. Mater.* **2025**, *35*, 2419809.
21 Xie, Z.; Dai, Y.; Wen, Y.; Zhang, M.; Tu, M.; Sun, F.; An, Z.; Zhao, T.; Liu, B.; Mao, Y. Hydrogel-based flexible degradable triboelectric nanogenerators for human activity recognition. *Sustainable Mater. Technol.* **2024**, *40*, e00967.
22 Zeng, X.; Teng, L.; Wang, X.; Lu, T.; Leng, W.; Wu, X.; Li, D.; Zhong, Y.; Sun, X.; Zhu, S. Efficient multi-physical crosslinked nanocomposite hydrogel for a conformal strain and self-powered tactile sensor. *Nano Energy* **2025**, *135*, 110669.
23 Hu, Y.; Zhang, M.; Qin, C.; Qian, X.; Zhang, L.; Zhou, J.; Lu, A. Transparent, conductive cellulose hydrogel for flexible sensor and triboelectric nanogenerator at subzero temperature. *Carbohydr. Polym.* **2021**, *265*, 118078.
24 Wang, S.; Zhang, Y. A functional triboelectric nanogenerator based on the LiCl/PVA hydrogel for cheerleading training. *Mater. Technol.* **2022**, *37*, 2752–2757.
25 Chen, Z.; Wang, K.; Fu, Y.; Zuo, Y.; Wei, M.; Xiong, J.; Wang, H.; Zhang, P.; Shang, N.; Zhong, D. Locking water molecules loss of PAA hydrogel for flexible zinc-air battery with NaCl doping. *Adv. Funct. Mater.* **2023**, *33*, 2306223.
26 Long, Y.; Zhang, Z.; Sun, K.; Wang, C.; Zeng, N.; Gao, B.; Tang, X.; Qi, X.; Fan, R. Enhanced electromagnetic wave absorption performance of hematite@ carbon nanotubes/polyacrylamide hydrogel composites with good flexibility and biocompatibility. *Adv. Compos. Hybrid Mater.* **2023**, *6*, 173.
27 Adhikari, B.; Banerjee, A. Short peptide based hydrogels: incorporation of graphene into the hydrogel. *Soft Matter* **2011**, *7*, 9259–9266.
28 Clasky, A. J.; Watchorn, J. D.; Chen, P. Z.; Gu, F. X. From prevention to diagnosis and treatment: Biomedical applications of metal nanoparticle-hydrogel composites. *Acta Biomater.* **2021**, *122*, 1–25.
29 Yang, T.; Yang, M.; Xu, C.; Yang, K.; Su, Y.; Ye, Y.; Dou, L.; Yang, Q.; Ke, W.; Wang, B. PEDOT: PSS hydrogels with high conductivity and biocompatibility for in situ cell sensing. *J. Mater. Chem. B* **2023**, *11*, 3226–3235.
30 Hou, R.; Xie, Y.; Song, R.; Bao, J.; Shi, Z.; Xiong, C.; Yang, Q. Nanocellulose/polypyrrole hydrogel scaffolds with mechanical strength and electrical activity matching native cardiac tissue for myocardial tissue engineering. *Cellulose* **2024**, *31*, 4247–4262.
31 Zhou, T.; Yuk, H.; Hu, F.; Wu, J.; Tian, F.; Roh, H.; Shen, Z.; Gu, G.; Xu, J.; Lu, B. 3D printable high-performance conducting polymer hydrogel for all-hydrogel bioelectronic interfaces. *Nat. Mater.* **2023,** *22*, 895–902.
32 Liu, D.; Huyan, C.; Wang, Z.; Guo, Z.; Zhang, X.; Torun, H.; Mulvihill, D.; Xu, B. B.; Chen, F. Conductive polymer based hydrogels and their application in wearable sensors: a review. *Mater. Horiz.* **2023**, *10*, 2800–2823.
33 Li, L.; Meng, J.; Zhang, M.; Liu, T.; Zhang, C. Recent advances in conductive polymer hydrogel composites and nanocomposites for flexible electrochemical supercapacitors. *Chem. Commun.* **2022**, *58*, 185–207.
34 Thirumalai, D.; Santhamoorthy, M.; Kim, S.-C.; Lim, H.-R. Conductive polymer-based hydrogels for wearable electrochemical biosensors. *Gels* **2024**, *10*, 459.
35 Sun, W.; Liu, X.; Hua, W.; Wang, S.; Wang, S.; Yu, J.; Wang, J.; Yong, Q.; Chu, F.; Lu, C. Self-strengthening and conductive cellulose composite hydrogel for high sensitivity strain sensor and flexible triboelectric nanogenerator. *Int. J. Biol. Macromol.* **2023**, *248*, 125900.
36 Wang, X.; Li, X.; Zhao, L.; Li, M.; Li, Y.; Yang, W.; Ren, J. Polypyrrole-doped conductive self-healing multifunctional composite hydrogels with a dual crosslinked network. *Soft Matter* **2021**, *17*, 8363–8372.
37 Cheng, Y.; Ren, X.; Duan, L.; Gao, G. A transparent and adhesive carboxymethyl cellulose/polypyrrole hydrogel electrode for flexible supercapacitors. *J. Mater. Chem. C* **2020**, *8*, 8234–8242.
38 Xu, H.; Li, Y.; Jia, M.; Cui, L.; Chen, C.; Yang, Y.; Jin, X. Design and synthesis of a 3D flexible film electrode based on a sodium carboxymethyl cellulose–polypyrrole@ reduced graphene oxide composite for supercapacitors. *New J. Chem.* **2021**, *45*, 6630–6639.
39 Cao, X.; Cao, Q.; Zhang, T.; Ji, W.; Muhammad, U.; Chen, J.; Wei, Y. Hydrophobically associated hydrogel for high sensitivity and resolution of an interdigital electrode pressure sensor. *Biomacromolecules* **2023**, *25*, 143–154.
40 Du, P.; Wang, J.; Hsu, Y.-I.; Uyama, H. Bio-inspired homogeneous conductive hydrogel with flexibility and adhesiveness for information transmission and sign language recognition. *ACS Appl. Mater. Interfaces* **2023**, *15*, 23711–23724.
41 Chafran, L.; Carfagno, A.; Altalhi, A.; Bishop, B. Green hydrogel synthesis: emphasis on proteomics and polymer particle-protein interaction. *Polymers* **2022**, *14*, 4755.
42 Basivi, P. K.; Ramesh, S.; Kakani, V.; Yadav, H.; Bathula, C.; Afsar, N.; Sivasamy, A.; Kim, H. S.; Pasupuleti, V. R.; Lee, H. Ultrasonication-mediated nitrogen-doped multiwalled carbon nanotubes involving carboxy methylcellulose composite for solid-state supercapacitor applications. *Sci. Rep.* **2021**, *11*, 9918.
43 Kulkarni, G.; Guha Ray, P.; Sunka, K. C.; Dixit, K.; Dhar, D.; Chakrabarti, R.; Singh, A.; Byram, P. K.; Dhara, S.; Das, S. Investigating the Effect of Polypyrrole–Gelatin/Silk Fibroin Hydrogel Mediated Pulsed Electrical Stimulation for Skin Regeneration. *ACS Appl. Mater. Interfaces* **2024**, *16*, 56762–56776.
44 Rao, L.; Liu, Y.; Zhu, S.; Zhong, G.; Wen, M.; Xu, K.; Yu, S.; Wang, S.; Niu, X. Flexible hydrogel-enhanced biomass loofah for efficient solar-driven interfacial evaporation. *Renew. Energy* **2026**, *256*, 123958.
45 Shi, Y.; Pan, L.; Liu, B.; Wang, Y.; Cui, Y.; Bao, Z.; Yu, G. Nanostructured conductive polypyrrole hydrogels as high-performance, flexible supercapacitor electrodes. *J. Mater. Chem. A* **2014**, *2*, 6086–6091.
46 Jeong, D.; Kim, C.; Kim, Y.; Jung, S. Dual crosslinked carboxymethyl cellulose/polyacrylamide interpenetrating hydrogels with highly enhanced mechanical strength and superabsorbent properties. *Eur. Polym. J.* **2020**, *127*, 109586.
47 Zheng, W. J.; Gao, J.; Wei, Z.; Zhou, J.; Chen, Y. M. Facile fabrication of self-healing carboxymethyl cellulose hydrogels. *Eur. Polym. J.* **2015**, *72*, 514–522.
48 Lin, F.; Lu, X.; Wang, Z.; Lu, Q.; Lin, G.; Huang, B.; Lu, B. In situ polymerization approach to cellulose–polyacrylamide interpenetrating network hydrogel with high strength and pH-responsive properties. *Cellulose* **2019**, *26*, 1825–1839.
49 Zhao, Y.; Wang, Z.; Wang, Y.; Cheng, Z. Mechanically resilient, freeze-resistant, and antibacterial carboxymethyl cellulose/phytic acid hydrogel sensors for respiratory monitoring. *Int. J. Biol. Macromol.* **2025**, *337*, 149374.
50 Yang, J.; Xu, F. Synergistic reinforcing mechanisms in cellulose nanofibrils composite hydrogels: interfacial dynamics, energy dissipation, and damage resistance. *Biomacromolecules* **2017**, *18*, 2623–2632.

51 Ding, Q.; Xu, X.; Yue, Y.; Mei, C.; Huang, C.; Jiang, S.; Wu, Q.; Han, J. Nanocellulose-mediated electroconductive self-healing hydrogels with high strength, plasticity, viscoelasticity, stretchability, and biocompatibility toward multifunctional applications. *ACS Appl. Mater. Interfaces* **2018**, *10*, 27987−28002.
52 Chen, C.; Li, Y.; Qian, C.; Liu, X.; Yang, Y.; Han, L.; Han, Q. Carboxymethyl cellulose assisted PEDOT in polyacrylamide hydrogel for high performance supercapacitors and self-powered sensing system. *Eur. Polym. J.* **2022**, *179*, 111563.
53 Zeng, H.; Zhang, L.; Wu, T.; Song, H.; Wan, Y.; Zhang, M. High-performance conductive hydrogel prepared by an electrohydrodynamic printing method for strain sensors and self-powered triboelectric nanogenerator. *ACS Appl. Nano Mater.* **2025**, *8*, 589−601.
54 Long, K.; Luo, Y.; Hu, C.; Xu, B.; Gu, X.; Ding, Z.; Guo, S. Anti-freezing, adhesive and conductive hydrogel for flexible sensors and deep learning assisted Triboelectric nanogenerators. *Chem. Eng. J.* **2025**, *513*, 162828.
55 Zhang, Y.; Chen, Z.; Zou, J.; Feng, P.; Jing, X. Sodium alginate supramolecular nanofibers in synergy with surface crack engineering to prepare tough and highly sensitive hydrogels. *Int. J. Biol. Macromol.* **2024**, *279*, 135507.
56 Liang, S.; Li, C.; Niu, M.; Zhu, P.; Pan, Z.; Mao, Y. Ionic hydrogels-based triboelectric nanogenerators for self-powered human−machine interfaces. *J. Phys.: Mater.* **2024**, *7*, 012001.
57 Hur, J.; Im, K.; Kim, S. W.; Kim, J.; Chung, D.-Y.; Kim, T.-H.; Jo, K. H.; Hahn, J. H.; Bao, Z.; Hwang, S. Polypyrrole/agarose-based electronically conductive and reversibly restorable hydrogel. *ACS Nano* **2014**, *8*, 10066−10076.
58 Peng, X.; Wang, W.; Yang, W.; Chen, J.; Peng, Q.; Wang, T.; Yang, D.; Wang, J.; Zhang, H.; Zeng, H. Stretchable, compressible, and conductive hydrogel for sensitive wearable soft sensors. *J. Colloid Interface Sci.* **2022**, *618*, 111−120.
59 Zhu, T.; Cheng, Y.; Cao, C.; Mao, J.; Li, L.; Huang, J.; Gao, S.; Dong, X.; Chen, Z.; Lai, Y. A semi-interpenetrating network ionic hydrogel for strain sensing with high sensitivity, large strain range, and stable cycle performance. *Chem. Eng. J.* **2020**, *385*, 123912.
60 Zhou, H.; Wang, M.; Jin, X.; Liu, H.; Lai, J.; Du, H.; Chen, W.; Ma, A. Capacitive pressure sensors containing reliefs on solution-processable hydrogel electrodes. *ACS Appl. Mater. Interfaces* **2021**, *13*, 1441−1451.
61 Wang, D.; Zhang, D.; Tang, M.; Zhang, H.; Sun, T.; Yang, C.; Mao, R.; Li, K.; Wang, J. Ethylene chlorotrifluoroethylene/hydrogel-based liquid-solid triboelectric nanogenerator driven self-powered MXene-based sensor system for marine environmental monitoring. *Nano Energy* **2022**, *100*, 107509.
62 Kanokpaka, P.; Chang, Y. H.; Chang, C. C.; Rinawati, M.; Wang, P.-C.; Chang, L. Y.; Yeh, M. H. Enabling glucose adaptive self-healing hydrogel based triboelectric biosensor for tracking a human perspiration. *Nano Energy* **2023**, *112*, 108513.

https://doi.org/10.1007/s10118-026-3681-y